ChemComm

Accepted Manuscript

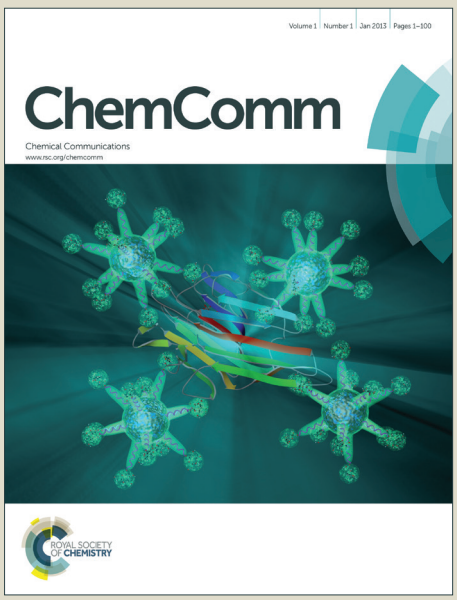

ROYAL SOCIETY OF CHEMISTRY

www.rsc.org/chemcomm

Journal Name

RSCPublishing

COMMUNICATION

Photoelectrochemical aptasensor for sensitive and selective detection of kanamycin based on Au nanoparticles functionalized self-doped TiO_2 nanotube arrays†

Cite this: DOI: 10.1039/x0xx00000x

Received 00th January 2012,
Accepted 00th January 2012

DOI: 10.1039/x0xx00000x

www.rsc.org/

Yanmei Xin, Zhenzhen Li, Zhonghai Zhang*

In this communication, a new photoelectrochemical aptasensor with Au nanoparticles functionalized self-doped TiO_2 nanotube arrays (Au/SD-TiO_2 NTs) as core sensing unit and aptamers as recognition unit was set up to accomplish the sensitive and selective detection of kanamycin with the lowest detection limit of 0.1 nM.

Kanamycin is an aminoglycoside antibiotic, produced by fermentation of Streptomyces kanamyceticus, and used in veterinary medicine to treat a wide variety of infections caused by Escherichia coli, Proteus, Enterobacter aerogenes, Klebsiella Pneumoniae, Serratia Marcescens, Acinetobacter spp and Staphylococcus through inducing mistranslation by interacting with the 30S subunit of the prokaryotic ribosome.[1] However, the widespread and overdosed using of kanamycin may cause its accumulation in the animal body and transfer in the food chain, thus lead to potential hazards to human health, such as damage of hearing and kidneys, allergic reactions and neurological symptoms.[2] The kanamycin contamination in animal-derived food was compulsory inspected in most countries, for example, the European Medicines Evaluation Agency has established the maximum residue limit of kanamycin in milk and in meat.[3] Currently, the detection methods for kanamycin was still based on complicated and expensive apparatus, such as high-performance liquid chromatography and capillary electrophoresis.[4] Therefore, it is desirable to establish a highly sensitive and selective sensing strategy for kanamycin detection.

Inspired from the photoelectrochemical (PEC) approach for solar energy conversion,[5] a new and promising PEC detection platform was recently proposed with high sensitivity due to its unique signal transducing modality, excitation energy sources of light and readout signal of electricity.[6] However, the exorbitantly high catalytic activity of the PEC materials would result in poor recognition of analytes, and thus limit its possibility for selective detection. While, if some terms of recognition units can be integrated into the PEC approach, a new detection platform with both high sensitivity and selectivity will be established. On this occasion, aptamers, single-stranded oligonucleotides with specific sequences, generated through an in vitro selection process of systemic evolution of ligands by exponential enrichment (SELEX), stood out as an effective recognition unit with the ability for rapid and accurate recognizing their cognate targets, such as ions, small biomolecules, proteins, and even cells, which have presented unprecedented advantages to traditional antibodies due to their high specificity, strong affinity, reusability and easy synthesis in vitro.[7] Herein, a new PEC aptasensor was proposed by integrated aptamers into the photoelectrode of gold nanoparticles (Au NPs) functionalized self-doped TiO_2 nanotube arrays (TiO_2 NTs) to realize the sensitive and selective detection of kanamycin. The TiO_2 NTs were rationally selected as pristine TiO_2 candidate due to its superior electron transportation stemmed from its unique one-dimensional nanotubular structures, and the Au NPs functionalized self-doped TiO_2 NTs (Au/SD-TiO_2 NTs) with the synergistic effect of surface plasmonic resonance from Au NPs and inter-bands from self-doped Ti^{3+} center, which would boost the PEC performance in visible light region.

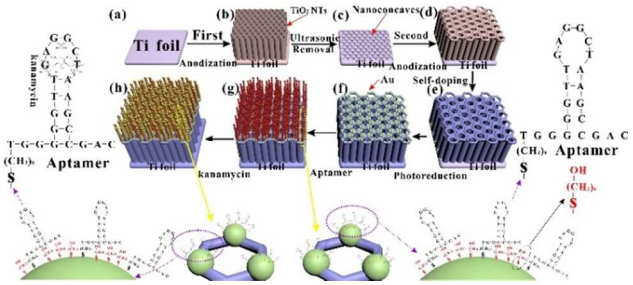

Fig. 1 Schematic diagram of the photoelectrochemical aptasensor. (a) Ti foil; (b) first-step anodized TiO_2 NTs; (c) Ti nanoconcaves; (d) second-step anodized TiO_2 NTs; (e) SD-TiO_2 NTs; (f) Au/SD-TiO_2 NTs; (g) aptamer-Au/SD-TiO_2 NTs; (h) kanamycin-aptamer-Au/SD-TiO_2 NTs.

The design and fabrication strategy of PEC aptasensor of aptamer-Au/SD-TiO_2 NTs is presented in Fig. 1. The TiO_2 NTs were fabricated in a facile two-step anodization process on the basis of our previous reported method with minor modification,[8] and the detailed experimental processes were presented in Experimental Section of ESI†. Briefly, a cleaned Ti foil (Fig. 1a) was first anodized in a fluoride contained organic electrolyte, then the as-grown TiO_2 NTs (Fig. 1b), with rough top surface (Fig. S1, ESI†), were thoroughly removed in an ultrasonic bath, whereas left behind well-ordered nanoconcaves on the Ti foil surface (Fig. 1c and Fig. S2, ESI†). The Ti foil with patterned nanoconcaves as template was subjected to a second anodization process to yield uniform TiO_2 NTs with unique

hierarchical top-porous-bottom-tubular nanostructures (Fig. 1d). Then, electrochemical reduction process (Fig. S3, ESI †) was conducted in supporting electrolyte of Na_2SO_4 solution under negative potentials of -1.5 V *vs* Ag/AgCl to induce self-doping center of Ti^{3+} into TiO_2 NTs (Fig. 1e).[9] Compared with hetero-doping, resulted in a deteriorated PEC performance by increasing the recombination center due to the foreign impurities, the self-doping with homo-species surface defect engineering strategy would be a more rational option to realize the enhancement of PEC performance.[10] Then, Au NPs were decorated on the SD-TiO_2 NTs in a photocatalytic reduction process to form Au/SD-TiO_2 NTs (Fig. 1f). The Au NPs owned dual functions in this case, one function was the enhancement of the PEC performance in visible light region as a sensitizer due to their surface plasmon resonance (SPR) activity,[11] and another function was the formation of the unique sulfur-gold linkage between the Au NPs and the mercapto group (HS-aptamer) to immobilize the aptamer on the surface of Au/SD-TiO_2 NTs (Fig. 1g). The mercapto group functionalized DNA aptamer (5'-HS-$(CH_2)_6$-TGGGG GTTGA GGCTA AGCCG A-3') was jointed on the Au NPs, and its secondary structure have been reported to bind the kanamycin into its loop region with high affinity and selectivity (Fig. 1h).[12] After the aptamer was attached on the Au NPs, mercaptohexanol was also introduced to cover the rest Au surface for voiding any nonspecifically adsorption of interferences. Thus, a PEC aptasenor for kanamycin detection was set up, and the bonded kanamycin would be recognized by the aptamer and oxidized by the photo-generated holes.

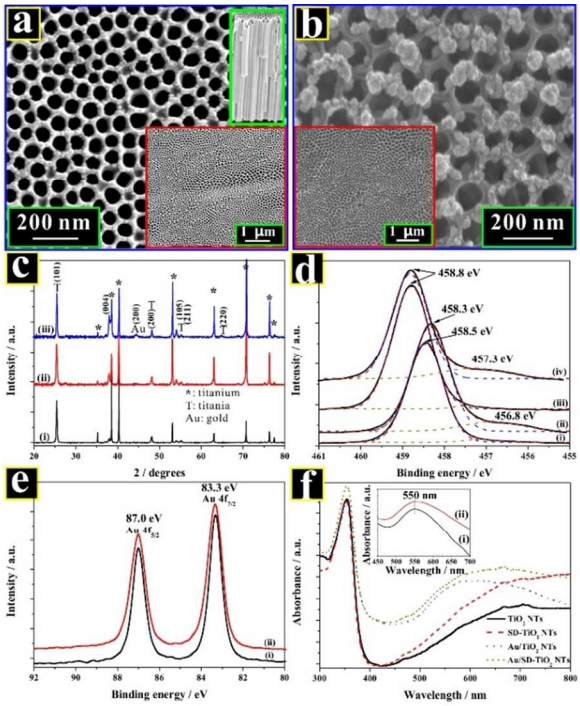

Fig. 2 (a) SEM image of high magnification top view of SD-TiO_2 NTs, the top inset is a cross-sectional view SEM image, and the bottom inset is a large scale top view SEM image; (b) SEM image of high magnification top view of Au/SD-TiO_2 NTs, the inset shows a large scale top view image; (c) XRD patterns of (i) TiO_2 NTs, (ii) SD-TiO_2 NTs, and (iii) Au/SD-TiO_2 NTs; high resolution XPS core level of (d) Ti 2p in (i) TiO_2 NTs, (ii) SD-TiO_2 NTs, (iii) Au/TiO_2 NTs, (iv) Au/SD-TiO_2 TNs, and (e) Au 4f in (i) Au/TiO_2 NTs, (ii) Au/SD-TiO_2 NTs; (f) diffuse reflectance UV-vis absorption spectra, the inset presents surface plasmon resonance absorption spectra of the Au NPs on the (i) Au/TiO_2 NTs and (ii) Au/SD-TiO_2 NTs.

The high magnification top view scanning electron microscope (SEM) image of SD-TiO_2 NTs was presented in Fig. 2a, which indicated a periodical top-nanopore structure with an average diameter of 70 nm. The high magnification SEM cross-sectional view (top-inset in Fig. 2a) helped to verify the hierarchical top-porous/bottom-tubular nanostructures and to identify the tube length of about 2 μm, which was rationally controlled to match the maximum penetration depth of the incident light in TiO_2 near the band gap. The bottom-inset in Fig. 2a depicted a large area SEM image of SD-TiO_2 NTs, which revealed a high uniformity of the top porous structure in large scale. Compared with the pristine TiO_2 NTs (Fig. S4, ESI†), the electrochemical reduction process did not significantly change the morphology and dimensions of the hierarchical nanotube structures. After photocatalytic reduction reaction, the Au NPs were uniformly decorated on the surface of SD-TiO_2 NTs with average size of 20 nm, as shown in Fig. 2b, no significant aggregation in large scale visible (inset of Fig. 2b). The energy dispersive X-ray spectroscopy (EDS) spectrum of the Au/SD-TiO_2 NTs supplied another evidence of the successful Au decoration (Fig. S5, ESI†).

The XRD patterns of the TiO_2 NTs, SD-TiO. NTs and Au/SD-TiO_2 NTs all showed dominant anatase phase with preferential orientation of (101) (Fig. 2c). The electrochemical reduction process did not change the crystal structure of SD-TiO_2 NTs. After Au NPs decoration, one obvious Au peak at 44.3° can be indexed to Au (200) plane. For further analyzing the chemical composition, oxidation states of titanium and understanding the interaction of Au NPs with SD-TiO_2 NTs, X-ray photoelectron spectroscopy (XPS) technique was employed (Fig. S6, ESI†). The high resolution core level spectra of Ti 2p are presented in Fig. 2d, a new peak with lower binding energy emerged after self-doping, as the formation of Ti^{3+} species,[13] and a slightly shift to lower energy of Ti^{4+} peak was observed due to the electrons transfer to the new forming neighbor Ti^{3+} center,[14] After the decoration of Au NPs, the Au/SD-TiO_2 NTs sample still presented an extra low energy binding peak at 457.3 eV, which implied that the photocatalytic deposition of Au NPs did not destroy the self-doping specie, in addition, both the Au/TiO_2 NTs and Au/SD-TiO_2 NTs samples presented a conversely positive shift to higher energy, which helped to confirm the electron transfer between oxygen vacancies of the TiO_2 and Au.[15] Moreover, the Au core level XPS spectra (Fig. 2e) presented two peaks at 83.3 and 87.0 eV for Au $4f_{7/2}$ and Au $4f_{5/2}$ respectively, which attributed to metallic gold, and the Au $4f_{7/2}$ showed a much lower binding energy than its bulk phase (84.0 eV), which also revealed the feasibility of the electron transfer between the Au and TiO_2 NTs.[16]

The UV-vis diffuse reflectance absorption spectra of TiO_2 NTs, Au/TiO_2 NTs, SD-TiO_2 NTs and Au/SD-TiO_2 NTs samples were measured and are presented in Fig. 2f. All samples showed strong UV absorption due to the electronic transition from the valence band to the conduction band. After self-doping process, the SD-TiO_2 NTs exhibited a remarkably enhanced absorption in whole visible light region as compared with the pristine TiO_2 NTs. The enhanced optical absorption can be attributed to the electronic transition from valence band to the inter-bands and/or from these inter-bands to the conduction band. The Au/TiO_2 NTs and Au/SD-TiO_2 NTs showed a significant visible absorption enhancement around 550 nm (inset in Fig. 2f), which can be ascribed to the SPR absorption of the Au NPs. The enhanced optical absorption from inter-bands overlapped with the wavelength of SPR of Au NPs, which would induce further light resonance and enhanced optical absorption. In fact, the Au/SD-TiO_2 NTs sample indeed presented higher SPR absorption than Au/TiO_2 NTs.

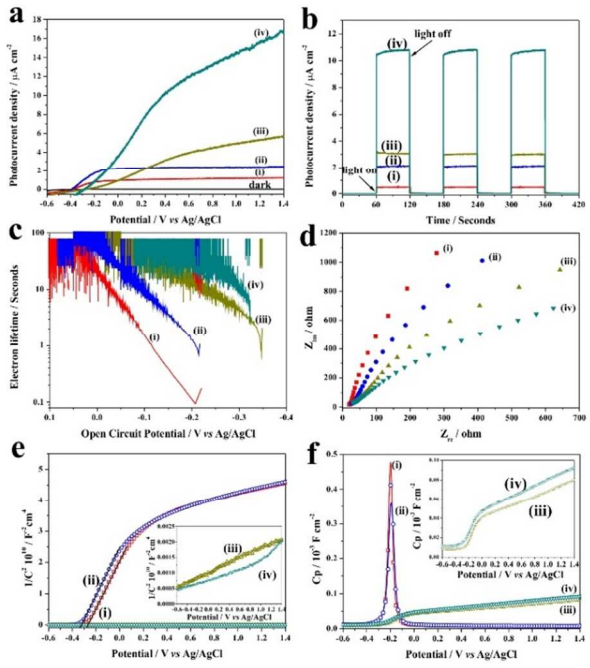

Fig. 3 Photoelectrochemical performance of (i) TiO_2 NTs, (ii) Au/TiO_2 NTs, (iii) SD-TiO_2 NTs, (iv) Au/SD-TiO_2 TNs in (a) linear-sweep voltammograms, collected with a scan rate of 5 mV s^{-1} under illumination of visible light with wavelength ≥420 nm; (b) amperometric transient photocurrent density *vs* time plots at an applied potential of 0.5 V *vs* Ag/AgCl under illumination of visible light with wavelength ≥420 nm with 60 s light ON/OFF cycles; (c) electron lifetime measurements determined from the decay of open circuit potential in dark; (d) electrochemical impedance spectra of Nyquist plots (Z_{re} *vs*. Z_{im}) under visible light illumination; (e) Mott-Schottky plots at a fixed frequency of 5 kHz in dark; (f) parallel capacitance (C_p) *vs* applied potential plots in a fixed frequency of 10 Hz in dark.

A series of PEC and electrochemical experiments were conducted to determine the PEC performance of TiO_2 NTs, Au/TiO_2 NTs, SD-TiO_2 NTs, and Au/SD-TiO_2 TNs samples under visible light illumination. Analysis of the linear sweep photovoltammograms (LSPV), as presented in Fig. 3a, allowed us to draw the following conclusions: (1) both Au/TiO_2 NTs, SD-TiO_2 NTs samples showed much enhanced photocurrent densities than TiO_2 NTs, which indicated that both the SPR from Au NPs and the inter-bands from self-doping created visible light response for TiO_2-based photoelectrode; (2) the Au/SD-TiO_2 TNs sample presented the highest photocurrent density among all the samples, and the significant enhanced photocurrent density was much higher than the increase from Au/TiO_2 NTs plus from SD-TiO_2 NTs samples, which implied the existence of synergistic effect between the Au NPs SPR and inter-bands induced from the self-doping process. Amperometric I-t measurements were also performed to examine the photo-response over time (Fig. 3b). All samples exhibited fast and reproducible photocurrent responses upon each illumination, and presented the same increased photocurrent density tendency as from LSPV measurements.

For further understanding the enhanced PEC performance, the inherent electronic properties were characterized by open-circuit photo-voltage decay (OCPVD), electrochemical impedance spectra (EIS) and capacitance measurements. The OCPVD experiments were performed and allowed us to estimate the photo-generated electron lifetime based on the following equation:[17]

$$\tau = \frac{k_B T}{e}\left(\frac{dV_{oc}}{dt}\right)^{-1} \quad (1)$$

where $\boldsymbol{\tau}$ is the potential dependent photoelectron lifetime, k_B is Boltzmann's constant, T is temperature, e is the charge of a single electron, and V_{oc} is the open-circuit voltage at time t. As shown in Fig. 3c, the Au/SD-TiO_2 TNs sample showed the longest electron lifetime, which contributed to its high PEC performances. The EIS is another powerful tool for studying the interfacial properties of photoelectrodes. Fig. 3d presented Nyquist plots under visible light illumination, and the Au/SD-TiO_2 TNs sample showed the smallest semicircle diameter, which indicated its smallest charge transfer resistance and fastest electron mobility. The capacitance measurement on the electrode/electrolyte was conducted to determine their carrier density (N_D) following the equation below:[18]

$$\frac{1}{C^2} = \frac{2}{N_D e \varepsilon_0 \varepsilon}\left[(U_S - U_{FB}) - \frac{k_B T}{e}\right] \quad (2)$$

where C is the space charge capacitance in the semiconductor; N_D is the electron carrier density; e is the elemental charge value; ε_0 is the permittivity of the vacuum; ε is the relative permittivity of the semiconductor; *Us* is the applied potential; *T* is temperature; and k_B is the Boltzmann constant. The carrier density N_D was determined from the Mott-Schottky (MS) plots as $1/C^2$ *vs* potential in Fig. 2e using the following equation: [18]

$$N_D = -\left(\frac{2}{e\varepsilon\varepsilon_0}\right)\left(\frac{d(1/C^2)}{d(U_s)}\right)^{-1} \quad (3)$$

with e = 1.6 × 10^{19}, ε_0 = 8.86×10^{-12} F/m, and ε = 48 for anatase TiO_2[19]. The calculate donor densities are 8.9×10^{17}, 9.2×10^{17}, 3.2×10^{20}, and 6.5×10^{20} cm^{-3} for TiO_2 NTs, Au/TiO_2 NTs, SD-TiO_2 NTs, and Au/SD-TiO_2 NTs, respectively. The significantly increased N_D confirmed that the self-doping process improved the electrical conductivity, accelerated the electron transfer. Fig. 3f showed the parallel capacitance (Cp) plotted against the applied potential. The TiO_2 NTs and Au/TiO_2 NTs samples presented obvious peaks at -0.2 V *vs* Ag/AgCl, which implied only one kind of surface defect, whereas, the SD-TiO_2 NTs and Au/SD-TiO_2 NTs samples presented continually increased capacitance value from -0.25 to 1.4 V *vs* Ag/AgCl, which indicated that the self-doping process created new types of surface defects.

The Au/SD-TiO_2 NTs sample was rationally selected as candidate of photoelectrode for PEC sensing measurements due to its best PEC performance under visible light illumination. After binding with the aptamer, the sensing performance of PEC aptasensor, aptamer-Au/SD-TiO_2 NTs, was well investigated and presented in Fig. 4. Fig. 4a presented the time-dependent PEC photocurrent (i-t) measurements with 0, 0.2 and 200 nM kanamycin, where the photocurrent density increased with the increase of the kanamycin concentrations, and the increased photocurrent density was mainly ascribed to the PEC oxidation of kanamycin from the photo-generated holes. The concentration of the aptamer was optimized and the experimental results were presented in Fig. S7, ESI†, and the photocurrent increased as the increase of the aptamer concentration till reached a steady state with the aptamer concentration of 2.5 μM, which concentration of aptamer was selected.

Chronoamperometry was applied to evaluate the sensitivity and detection range of the PEC aptasensor, and the photocurrent response upon the addition of kanamycin was presented in Fig. 4b. With the addition of kanamycin with different concentrations, the photocurrent rapidly increased and rapidly reached a steady state. Based on a signal-to-noise factor of 3 (S/N = 3), the detection limit can be calculated to be 0.1 nM (inset in Fig. 4b). The calibration curve of photocurrent density *vs* kanamycin concentrations was shown in Fig. 4c, and the curve exhibited a good linear relationship in the ranges of 0.2-200 nM (R^2 = 0.9987, sensitivity = 0.0268 μA cm^{-2} nM^{-1}), which was much sensitive than the PEC aptasensor fabricated by aptamer-Au/TiO_2 NTs (R^2 = 0.9985, sensitivity = 0.0088 μA cm^{-2} nM^{-1}, Fig. S8, ESI†). Compared with the previously

reported kanamycin aptasensor, this rationally designed PEC aptasensor presented the lowest detection limit and large detection range (Table S1, ESI†).

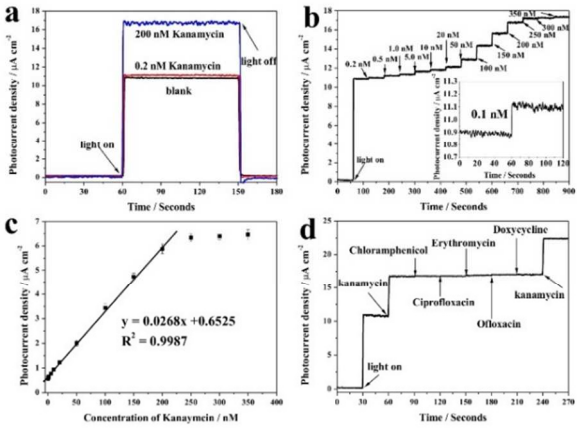

Fig. 4 (a) Amperometric transient photocurrent density vs time plots at an applied potential of 0.5 V *vs* Ag/AgCl under illumination of visible light with wavelength ⩾420 nm with light ON/OFF model for 0, 0.2 and 200 nM kanamycin; (b) Photocurrent density vs time for successive addition of kanamycin at 0.5 V *vs* Ag/AgCl under illumination of visible light with wavelength ⩾420 nm, the right-bottom inset is the magnified image of the first 120 seconds of the sensing curve; (c) photocurrent density-kanamycin concentration calibration curve; (d) anti-interference property with initial addition of 100 nM kanamycin and 100 nM of chloramphenicol, ciprofloxacin, erythromycin, ofloxacin, doxycycline, followed by addition of another 100 nM kanamycin.

The selectivity of the PEC aptasensor was demonstrated by measuring the photocurrent response upon the addition of different molecular interferences. As shown in Fig. 4d, the addition of 100 nM of kanamycin resulted in a quick and significant photocurrent increase, whereas an addition of 100 nM of chloramphenicol, ciprofloxacin, erythromycin, ofloxacin, doxycycline did not cause observable photocurrent changes, after that, another 100 nM kanamycin was added and an obvious photocurrent increase was observed again. In this PEC aptasensor, the aptamer was used as recognition unit, and the Au/SD-TiO_2 NTs was used as sensing unit, where the kanamycin was caught by the aptamer, and oxidized by the photo-generated holes from Au/SD-TiO_2 NTs. However, the interferences of ciprofloxacin, erythromycin, ofloxacin, doxycycline cannot be captured by the aptamer, and cannot reach the surface of the photoelectrode due to the steric effect as all the surface of Au NPs were occupied by the aptamer and the mercaptohexanol as blocking agent. Thus the PEC aptasensor possessed a very favorable selectivity toward kanamycin detection.

The detection reproducibility was also investigated by measuring the response photocurrent of more than five aptasensors, and a standard deviation of 3.75% was achieved, confirming the good reproducibility. In addition, the long-term stability of the aptasensors were also tested by studying the current response intermittently in a period of 30 days (stored at 4 °C after the each measurements), and no obvious photocurrent differences were found, suggesting the aptasensor was quite stable for the kanamycin sensing.

The PEC aptasenosr was used to detect the recoveries of different concentrations of kanamycin in commercial-available bovine milk by standard addition method to evaluate its feasibility of detection of real samples. The results were shown in Table S2, ESI†, and the recovery was in the range of 94.8-103% with low relative standard deviation in the range of 2.31-3.15%, which results were consistent with the data from enzyme-linked immunosorbent assay (ELISA) analysis, and thus revealed that the PEC aptasenosr can be utilized for determining of kanamycin in animal derived foods.

In summary, we set up a new PEC aptasensor with Au NPs functionalized self-doped TiO_2 NTs as core sensing unit and aptamers as recognition unit to accomplish the sensitive and selective detection of kanamycin with the lowest detection limit. In addition, the synergistic effect between SPR from the Au NPs and inter-bands from the self-doping induced Ti^{3+} centre boosted the PEC performance under visible light irradiation, which paved a new avenue not only for designing of sensitive PEC sensors but also exploiting its PEC applications for solar energy conversion.

We thank to the support from "Yingcai" program of ECNU, Shanghai Pujiang Program (14PJ1403400), and National Natural Science Foundation of China (No. 21405046).

Notes and references

School of Chemistry and Molecular Engineering, East China Normal University, 500 Dongchuan Road, Shanghai 200241, China.
Address correspondence to zhzhang@chem.ecnu.edu.cn

† Electronic Supplementary Information (ESI) available: Experimental details, SEM images, EDX spectrum, XPS survey, additional electrochemical data. See DOI: 10.1039/c000000x/

1 (a) J. W. Park, S. R. Park, K. K. Nepal, A. R. Han, Y. H. Ban, Y. J. Yoo, E. J. Kim, E. M. Kim, D. Kim, J. K. Sohng, Y. J. Yoon, *Nat. Chem. Biol.* **2011**, 7, 843; (b) J. Wirmer, E. Westhof. *Methods. Enzymol*. **2006**, 415, 180.
2 (a) R. C. Atkins, C. Mion, E. Despaux, N. Van-Hai, C. Julien, H. Mion, *Kidney. Int*. **1973**, 3, 391; (b) S. Yu, Q. Wei, B. Du, D. Wu, H. Li, L. Yan, H. Ma, Y. Zhang, *Biosens. Bioelectron*. **2013**, 48, 224.
3 European Commission Regulation (EU) No. 37/2010, Off. J. Eur. Union, **2010**, L15, 1.
4 (a) B. Blanchaert, E. Poderós Jorge, P. Jankovics, E. Adams, A. van Schepdael *Chromatographia* **2013**, 76, 1505-1512; (b) M. N. El-Attug, E. Adams, J. Hoogmartens, A. van Schepdael, J. *Sep. Sci*. **2011**, 34, 2448.
5 (a) A. Fujishima, K. Honda, *Nature* **1972**, 238, 37; (b) F. E. Osterloh, *Chem. Soc. Rev*. **2013**, 42, 2294; (c) Q. Liu, J. He, T. Yao, Z. Sun, W. Cheng,S. He, Y. Xie, Y. Peng, H. Cheng, Y. Sun, Y. Jiang, F. Hu, Z. Xie, W. Yan, Z. Pan, Z. Wu, S. Wei, *Nat. Commun*. **2014**, 5, 5122.
6 (a) W. W. Zhao, J. J. Xu, H. Y. Chen, *Chem. Rev*. **2014**, 114, 7421; (b) W. W. Zhao, J. J. Xu, H. Y. Chen, *Chem. Soc. Rev*. **2015**, 44, 729.
7 (a) D. S. Wilson, J. W. Szostak, *Annu. Rev. Biochem*. **1999**, 68, 611; (b) S. D. Jayasena, *Clin. Chem*. **1999**, 45, 1628; (c) C. Tuerk, L. Gold, *Science* **1990**, 249, 505; (d) A. D. Ellington, J. W. Szostak, *Nature* **1990**, 346, 818; (e) X. Fang, W. Tan, *Acc. Chem. Res*. **2010**, 43, 48.
8 Z. Zhang, P. Wang, *Energy Environ. Sci*. **2012**, 5, 6506.
9 Z. Zhang, M. N. Hedhili, H. Zhu, P. Wang, *Phys. Chem. Chem. Phys*. **2013**, 15, 15637-15644.
10 Z. Zhang, X. Yang, M. N. Hedhili, E. Ahmed, L. Shi, P. Wang, *ACS Appl. Mater. Interfaces* **2014**, 6, 691.
11 P. Da, W. Li, X. Lin, Y. Wang, J. Tang, G. Zheng, *Anal. Chem*. **2014**, 86, 6636.
12 (a) K. M. Song, M. Cho, H. Jo, K. Min, S. H. Jeon, T. Kim, M. S. Han, J. K. Ku, C. Ban, *Anal. Biochem*. **2011**, 415, 175; (b) X. Sun, F. Li, G. Shen, J. Huang, X. Wang, *Analyst* **2014**, 139, 299.
13 Q. Kang, J. Cao, Y. Zhang, L. Liu, H. Xu, J. Ye, *J. Mater. Chem. A* **2013**, 1, 5766.
14 M. C. Biesinger, L. W. M. Lau, A. R. Gerson, R. St. C. Smart, *Appl. Surf. Sci*. **2010**, 257, 887.
15 Z. Zhang, L. Zhang, M. N. Hedhili, H. Zhang, P. Wang, *Nano. Lett*. **2013**, 13, 14.
16 J. C. Fuggle, N. Mårtensson, *J. Electron Spectrosc. Relat. Phenom*.**1980**, 21, 275.
17 B. H. Meekins, P. V. Kamat, *ACS Nano* **2009**, 3, 3437.
18 G. Wang, Q. Wang, W. Lu, J. Li, *J. Phys. Chem. B* **2006**, 110, 22029.
19 P. K. Ghosh, M. E.Azimi, *IEEE Trans. Dielectr. Electr. Insul*. **1994**, 1, 975.

Graphic Abstract

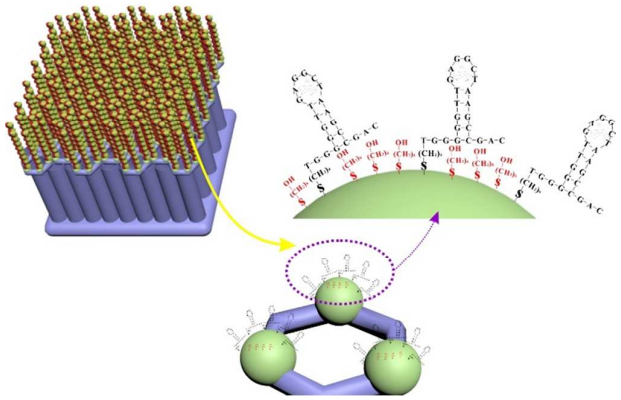

A new photoelectrochemical aptasensor with Au nanoparticles functionalized self-doped TiO_2 nanotube arrays as core sensing unit and aptamers as recognition unit was set up to accomplish the sensitive and selective detection of kanamycin.